Electronic structure and optical properties of WO_3, $LiWO_3$, $NaWO_3$, and HWO_3

Anders Hjelm and Claes G. Granqvist
Department of Technology, Uppsala University, Box 534, S - 751 21 Uppsala, Sweden

John M. Wills
Theoretical Division, Los Alamos National Laboratory, Los Alamos, New Mexico 87544

(Received 2 January 1996)

The electronic structures for cubic WO_3, $LiWO_3$, $NaWO_3$, HWO_3, H_2WO_3, and hexagonal WO_3 have been calculated. The calculations rely on the local approximation to density functional theory and use a full-potential linear muffin-tin orbitals method. The incorporation of ions in tungsten oxide by chemical or electrochemical methods is the basis for several technological applications related to solid state ionics. Essentially, incorporation of alkali ions results in an *s*-band high above the Fermi level, and the charge-balancing electrons take part in a rigid band filling of the W *d* conduction band. Hydrogen forms a hydroxide unit with one oxygen atom, and we find a minimum in total energy for a bond length of 1.03 Å . The cubic phase of WO_3 can take up more than one hydrogen atom, and the formation of two hydroxide units is preferable to one water molecule. The calculated dielectric function and reflectance of Li_xWO_3 and Na_xWO_3 are presented, and the change in optical properties being the basis for reflective electrochromism is reproduced, although the reflectance curves show some deviations from experiments.
[S0163-1829(96)11027-4]

I. INTRODUCTION

The optical properties of tungsten-oxide-based materials have been the subject of scientific curiosity for almost two centuries. While stoichiometric WO_3 is yellowish to greenish in bulk form, it is possible to produce strong color changes by passing hydrogen over gently warmed WO_3 as noted by Berzelius already in 1815.[1] A striking goldlike appearance was reported by Wöhler[2] in 1824 for Na-containing WO_3. More recent work has been oriented towards studies of the optical properties as a function of quantitative hydrogen or alkali ion content; a fairly complete description of the optical properties of Na_xWO_3 was given by Brown and Banks.[3] The visual appearance goes from greenish—through gray, blue, purple, red, and orange—to yellow as x is increased from zero to unity.[4] Electrochemical treatment of WO_3 offers convenient possibilities to modify its optical properties. Reduction in an acidic electrolyte yielded a blue material, as reported in 1930 by Kobosew and Nekrassow,[5] and reversible color changes during electrochemical polarization of Na_xWO_3 were mentioned in 1951 by Brimm *et al.*[6]

During the past 25 years it has become increasingly apparent that WO_3, modified by ion incorporation or substoichiometry, can exhibit many technologically important properties. First and foremost one can achieve electrochromism, i.e., optical properties that can be modified reversibly and persistently by electrical pulses.[7,8] Electrochromism relies on combined ion and electron insertion and/or extraction in materials in contact with an electrolyte or ion conductor. Electrochromic WO_3-based devices[7,8] are currently being developed for ''smart windows'' with variable throughput of visible light and solar energy, high contrast systems for passive and active information display, variable-reflectance mirrors, and variable emittance surfaces for controlled thermal emission. It is also possible to vary the optical properties of WO_3 by dc current injection, ultraviolet irradiation, exposure to atomic hydrogen or to H_2 gas in contact with a catalyst, irradiation by a beam of ions or electrons, or heating.[7]

An in-depth investigation of the electronic structure of ion-containing WO_3 is amply justified because of its relevance for new and emerging technology, as noted above, and such a study is of much interest also from a fundamental perspective. Previous studies on the electronic structure of WO_3 and related materials have been performed by several different groups. The position of the oxygen and metal *d* bands as well as crystal field effects were investigated by Mattheiss in 1970.[9] The first specific calculation for WO_3, together with $NaWO_3$, was performed by Kopp *et al.* in 1977, using the cubic structure. Bullett showed in 1983 that the distortion of the lattice to a monoclinic structure increases the band gap.[10] A detailed study of Na_xWO_3 for various values of x was presented by Zhan and Zheng in 1993.[11] All of these calculations were based on atomic charge densities or wave functions, and thus were not self-consistent. To our knowledge the only self-consistent calculation performed previously for WO_3-related materials was by Christensen and Mackintosh,[12] for $NaWO_3$. Christensen and Mackintosh point out that self-consistency is important in calculations for materials with large charge transfer between the atoms like tungsten-based oxides. Furthermore, the crystal structures of the WO_3-related materials are extremely open, and several calculational techniques such as the atomic spheres approximation have difficulties in handling open structures. In the present work we employ a full-potential method, where openness does not cause any complications, in order to study the electronic structure of WO_3-based materials.

The following section (Sec. II) describes the calculational technique. In Sec. III we present the calculated electronic

structures for pure WO_3 in the cubic and hexagonal phases, and for $LiWO_3$, $NaWO_3$, and H_xWO_3 with x being 1 and 2. Section IV presents the calculated optical properties of Li_xWO_3 and Na_xWO_3, which are of much interest for applications to reflective electrochromic devices. Finally, in Sec. V we discuss and summarize the theoretical results obtained.

II. CALCULATIONAL METHOD

The band structures were calculated fully self-consistently using the local density approximation (LDA) to density functional theory (DFT).[13] The exchange-correlation potential was represented according to von Barth and Hedin with parameters given by Janak *et al.*[14] Basis functions and matrix elements were constructed using a full-potential linear muffin-tin orbital method (FP-LMTO).[15] The charge density and potential were expanded in symmetry-adapted spherical harmonics, truncated at $l=8$, in a muffin-tin sphere around each atomic site. The spheres were nonoverlapping, and in the interstitial region the charge density and potential were expanded in 24^3 Fourier waves. The basis set consisted of augmented linear muffin-tin orbitals.[16] The tails of the basis functions outside their parent spheres were linear combinations of Hankel or Neuman functions with nonzero kinetic energy. Tungsten site centered 5p, 6s, 6p, and 5d wave functions were used, and 2s and 2p functions centered on oxygen sites. When H, Li, or Na were included in the calculations, the s and p functions with appropriate principal quantum number were employed. A double basis set was used, i.e., two basis functions of the same quantum numbers were taken to be connected to tails with different kinetic energy. Furthermore, the W 5p constituted a pseudovalence state and used tail energies considerably lower than those of the true valence wave functions, although fully hybridizing with the valence states. Relativistic effects were treated in the scalar relativistic approximation,[17] i.e., spin-orbit coupling was not included. The core states were relaxed in each iteration, using a fully relativistic equation.

The Brillouin zone integrations used a special point method with Gaussian smearing over a width of 1 mRy.[18] In all calculations, except those for the hexagonal structure, a **k**-point density corresponding to 56 points in $\frac{1}{48}$ of the cubic Brillouin zone was adopted. Fifty points were used for the hexagonal phase.

WO_3 and related materials can be found in a large variety of crystal structures.[7] The tungsten oxides consist of WO_6 octahedra arranged in various corner-sharing or edge-sharing configurations.[7,19] The simplest form is the defect perovskite or ReO_3 structure shown in Fig. 1. The figure also illustrates the positions of intercalated ions occupying symmetry positions; clearly a perovskite structure is then formed. Pure, bulky WO_3 does not generally exist in a cubic structure, but instead a monoclinic phase appears to be most stable at room temperature.[20] In thin films, however, it is most likely that the octahedra are ordered hexagonally in crystallites with sizes depending on the fabrication route and deposition temperature.[21] The monoclinic phase requires a large unit cell (containing eight W atoms) and hence too much computing power, and we have therefore chosen to study the cubic structure as a model system. However, it is the ubiquitous octahedral order that dominates the electronic properties, and this approximation thus should be adequate. We also illuminate the differences in the electronic structure caused by various structures as we have performed calculations for the hexagonal phase, which requires three W atoms per unit cell.

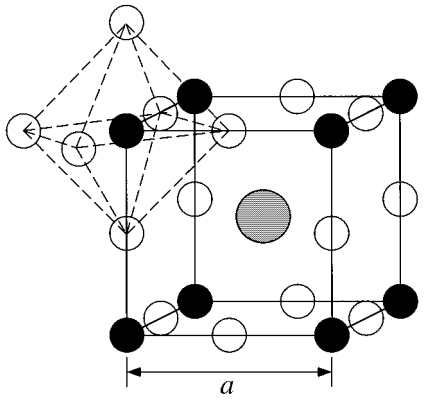

FIG. 1. Perovskite crystal structure for (Li,Na)WO_3 with tungsten atoms as solid circles, oxygen atoms as empty circles, and Li or Na atoms as a dashed circle. The ReO_3 structure, used as an approximation for monoclinic WO_3, corresponds to omission of the Li or Na site. The lattice constant a is defined and the octahedron, built up by oxygen atoms, surrounding the tungsten atom is shown.

Intercalation of H, Li, or Na in WO_3 leads to intricate structural changes that are not yet fully understood. Cubic structures have been reported for $H_{0.5}WO_3$, Li_xWO_3 with $0.1<x<0.4$, and Na_xWO_3 with $0.3<x<1$. The Li and Na atoms are expected to lie at the centers of the perovskite units (cf. Fig. 1), whereas the H atoms are significantly off-center and are attached to oxygen atoms in hydroxyl groups.[22] Further details, as well as references to the extensive literature on structural matters, can be found in Refs. 4, 7, and 23. Our computations of electronic structure were confined to cubic HWO_3, $LiWO_3$, and $NaWO_3$.

III. ELECTRONIC STRUCTURES

A. Cubic WO_3

The highest occupied atomic energy levels of oxygen and tungsten atoms can be estimated by their first ionization potentials, 13.6 eV and 8.0 eV, respectively. These energies, together with the Madelung energy, can give a hint to where the center of the corresponding energy bands can be found in the solid. The widths of the bands are more difficult to estimate, since they depend on the amount of W-W and O-O wave function overlap. Furthermore, W-O hybridization affects the actual bandwidth. The oxygen bands (originating from the three atoms in the unit cell) can accommodate 18 electrons, while the oxygen atoms only contribute with 4 electrons each. Since the W d states are approximately 5 eV higher in energy, it is very likely that the 6 tungsten valence electrons are transferred to the oxygen p bands, which thus will be completely filled. If the bandwidths are sufficiently small, the material will be a semiconductor with O p states below the band gap and W d above.

The calculated density of states (DOS) for WO_3 is presented in Fig. 2. Indeed, the material is a semiconductor, in agreement with experiments.[7] The O 2p and W 5d projected

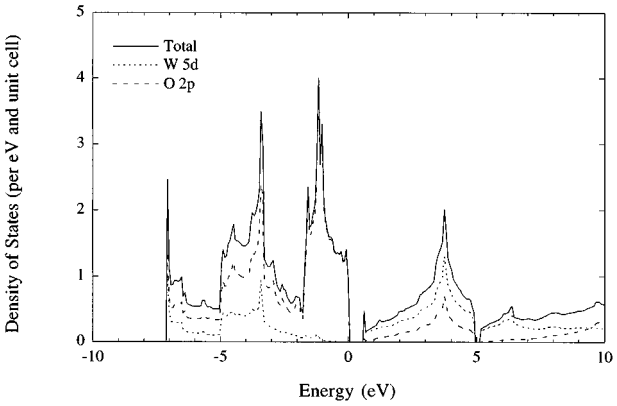

FIG. 2. Density of states for cubic WO_3. Filled states are found at energies below zero and empty states above. Also shown are the O $2p$ and W $5d$ projected state densities.

contributions to the total DOS are included in the figure. The graph shows that, as expected, the valence band is dominated by the O p states, while W d states dominate the conduction band. In addition, there is considerable hybridization between the valence and conduction bands. The O $2s$ levels are not included in the figure; they are positioned at -17.5 eV. The calculated band gap is quite small, 0.6 eV compared to the experimentally determined value of 2.6 eV for the indirect band gap.[7] This difference points to a common failure when the LDA is applied to semiconducting systems.[24] Furthermore, the approximation of the crystal structure (cubic) used in the present work seems to reduce the band gap compared to that of the experimentally found structures.[10]

The calculated total energy of cubic WO_3 displays a minimum for a lattice constant of 3.84 Å. Since this structure is not found in nature it is impossible to make a direct comparison with experimental data, but the ''average'' lattice constant in monoclinic WO_3, being the structure which most resembles the cubic and also is found at room temperature, is 3.75 Å. Na_xWO_3 is cubic and single-phase for $x>0.5$, and a linear extrapolation to $x=0$ gave a lattice constant of 3.78 Å.[3] Thus the calculated equilibrium volume is in good agreement with experiment.

The charge density in cubic WO_3 is presented in Figs. 3(a) and 3(b), where the former shows the charge density in a (100) plane cutting through the basal plane of the structural unit cell shown in Fig. 1 and the latter refers to the (100) plane with $z=a/2$, where z is the coordinate along the (001) axis, found in the middle of the cube shown in Fig. 1. In Fig. 3(a) W sites are located at the corners and O sites at the midpoints of the edges, while in Fig. 3(b) four O atoms are found at the corners. The two charge density plots reveal the openness of the defect perovskite structure; the charge density is approximately zero except for quite small regions around the atomic sites, where the charge density appears to be spherical. A considerable amount of charge is found around the W sites, originating from the pseudovalence $5p$ states, but also from the conduction electrons. The latter part of the density demonstrates that the material is not ionic; instead the transfer of the W valence electrons to lower lying energy bands is mediated by the W-O hybridization.

In order to investigate the amount of covalency, Fig. 4 displays the charge density with the spherically symmetric

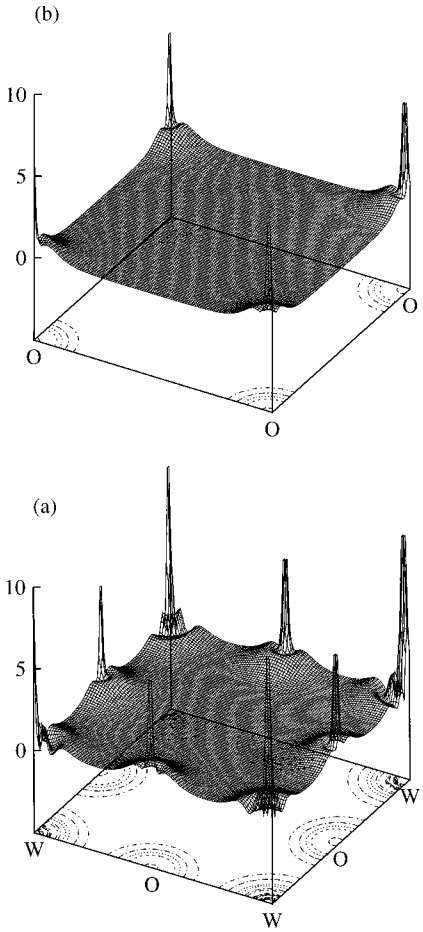

FIG. 3. Charge density of WO_3 in the plane $z=0$ (a) (lower panel) and in the plane $z=a/2$ (b) (upper panel) with a being the perovskite lattice parameter. In (a) the tungsten sites are at the corners and the oxygen sites on the edges (cf. Fig. 1). In (b) the oxygen sites are found at the corners.

component subtracted for the same cuts through the unit cell as in Fig. 3. It is important to notice that the vertical scale in Fig. 4 is 200 times smaller than the scale in Fig. 3, implying that the covalent contribution is very small. The anisotropy that can be observed shows that the W density points towards the nearest oxygen atom, as expected from the large tungsten-oxygen hybridization in the valence band. Charge-density lobes in this direction resemble e_g states, while one normally would expect t_{2g} states to have lower energy. But the present W d occupation comes solely from hybridization between the tungsten and oxygen atoms, and consequently the charge distribution behaves similarly to e_g-like states. In the (unoccupied) conduction band the t_{2g} orbitals have the lowest energy. The oxygen density points towards the nearest neighbor but also has a lobe in the direction perpendicular to the W-O bond direction.

The charge distribution is summarized in Table I where the occupation numbers of the l-projected orbitals within each sphere are given. In interpreting these numbers one must, however, remember that they are dependent on the sizes of the muffin-tin spheres. For the present case, the W sphere constitutes 11% of the volume, one O sphere 3.3%, and the interstitial region 79% of the total volume.

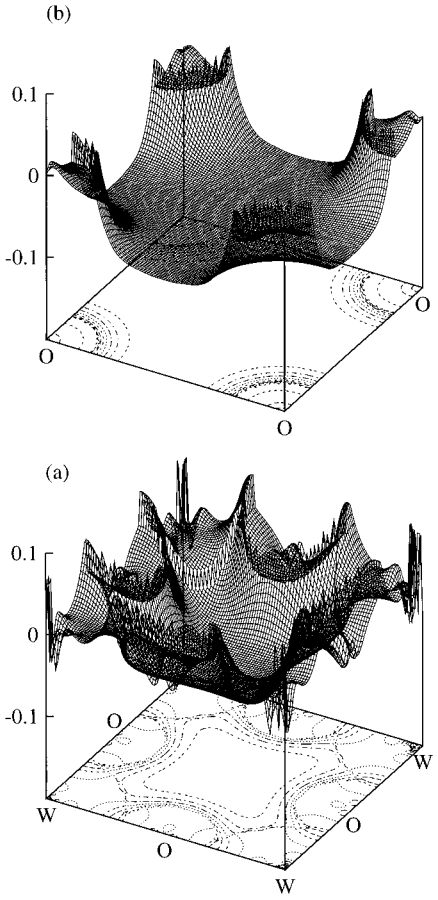

FIG. 4. Charge density of WO_3 with the spherically symmetric components subtracted in the plane $z=0$ (a) (lower panel) and in the plane $z=a/2$ (b) (upper panel) with a being the perovskite lattice parameter. Atomic sites are the same as in Fig. 3.

B. Hexagonal WO_3

In thin films made by several different techniques, many of the WO_6 octahedra are hexagonally coordinated.[7,21] At an appropriately high substrate temperature for the film growth or at suitable annealing temperature, the structure may be almost ''bulk'' hexagonal. Hexagonal clusters are formed at lower temperatures, with smaller cluster size at diminished temperature. Certainly finite-size properties of the clusters, and the mechanisms involved in the bonding between the clusters, are important for the macroscopic properties of the material. Nevertheless, the possibility to investigate the differences between the cubic and hexagonal phases is important, and we present the calculated electronic structure also for hexagonal WO_3.

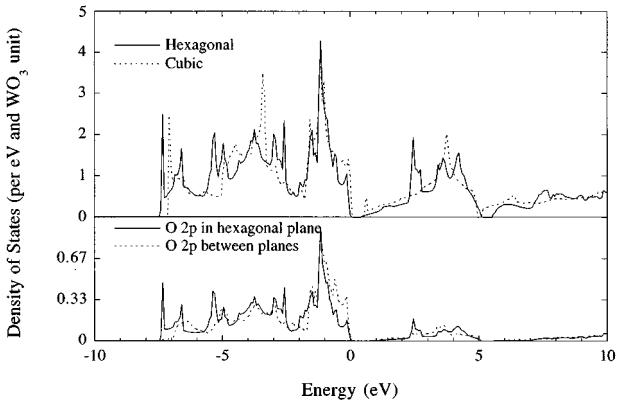

FIG. 5. Density of states for hexagonal WO_3 together with cubic WO_3 (upper panel), and oxygen projected density of states in the hexagonal structure for oxygen atoms in the basal plane ($z=0$) or at $z=c/2$, where c is the length of the symmetry axis in the hexagonal unit cell (lower panel).

Lattice parameters of bulk hexagonal WO_3 have been estimated by Figlarz,[19] who showed that two hexagonal phases exist, one hydrated where the hexagonal layers of WO_6 octahedra are shifted from one layer to another, and one dehydrated (after annealing) where the hexagonal layers are stacked directly on top of each other. We have chosen to study the latter phase, which is advantageous since it is the least complex structure with three WO_3 units per unit cell. All W-O distances are equal in the basal plane (following the hexagonal symmetry), while the W-O distance along the c axes is slightly larger.[19]

The calculated density of states for the hexagonal phase of WO_3 is presented in Fig. 5 together with the DOS for the cubic phase (upper panel). Also reported is the oxygen p projected density for one of the six atoms in the basal plane

TABLE I. Calculated and experimental lattice constants a and occupation number for the tungsten oxide and tungsten bronzes. Lattice constant given in italics means that direct comparison between theory and experiment is not possible, but the value is an estimate based on other structures.

	Lattice constant (Å)		Occupation number per site					
Material	theor.	expt.	Wd	Wsp	Os	Op	ion	interstitial
WO_3	3.84	*3.78*	2.27	0.34	1.45	3.22	-	7.23
$LiWO_3$	3.88	*3.71*	2.46	0.34	1.44	3.25	0.13	7.83
$NaWO_3$	3.88	3.87	2.46	0.34	1.44	3.26	0.10	7.84
HWO_3 [a]	3.83	-	2.31	0.33	1.45	3.21	0.75	7.46
HWO_3 [b]	-	*3.78*	2.47	0.34	1.44/0.65 [c]	3.21/1.66 [c]	0.43	10.0

[a]With hydrogen in the central position ($d_{OH}=2.71$ Å), not spin polarized.
[b]With hydrogen in the position giving the total energy minimum, $d_{OH}=1.03$ Å .
[c]The smaller values correspond to the oxygen sphere in the hydroxide unit, which has a shorter radius than the other oxygen spheres.

and one of the three oxygen atoms between the planes, representing the largest differences between the oxygen sites.

The detailed shapes of the DOS for the two structures are different, of course. The most important differences between hexagonal and cubic WO_3 is that the bottom of the conduction band shows a much smoother onset above the gap in the hexagonal structure while the cubic phase has a peak at this position. The width of the O p bands is somewhat broader in the hexagonal phase than in the cubic, and it is interesting that the O $2p$ density is quite different for the oxygen atoms in and between the hexagonal planes (lower panel). The states originating from the atoms in the plane dominate in the low energy part of the band, while the states corresponding to the sites between the planes dominate the top of the oxygen p band. The band gaps are roughly of equal magnitude in the two calculations, but as pointed out earlier, the band gaps are difficult to estimate within the LDA. The splitting between the t_{2g} and e_g components of the W d bands appears at a slightly higher energy in the hexagonal structure, and the gap is slightly larger.

The total energy calculated for the cubic and hexagonal structures differs by 0.1 Ry, where the cubic structure has the lowest energy. This is consistent with the fact that the monoclinic phase of WO_3 is the normal one when the material is in bulk form. When the material grows under evaporation, sputtering, or sol-gel deposition hexagonal ordering is preferred,[7,21] and a detailed understanding of the deposition energetics and the growth process is needed in order to grasp the structural formation.

The present study strongly supports the view that the octahedral ordering in WO_3 dominates its electronic properties, and confining the following studies in this paper to the simpler cubic structure is very likely to provide insights into the electronic structure in real materials.

C. $LiWO_3$

When lithium ions are inserted into the tungsten oxide crystal, either at the fabrication or by electrochemical posttreatment, dramatic differences are observed in the electronic properties. The material goes from semiconducting to metallic. This can be understood from the energy of the atomic Li $2s$ level, which is 5.4 eV, above the W $5d$ level. The Li band thus is likely to be positioned high up in the conduction band, whereas the associated electron will occupy the lowest empty state at the bottom of the conduction band. Hence the material will be metallic with W $5d$ bands at the Fermi level.

Figure 6 presents the calculated DOS. The Li $2s$ band is centered at 8.2 eV above the top of the valence band, and the Fermi level is found at 2.9 eV, in the conduction band. This gives a very low occupation of the Li band, as seen in Table I; it is only 0.13 electrons. (For the present calculation the volume of the W, O, and Li spheres and the interstitial region is 11%, 3.3%, 11%, and 68% of the total volume, respectively; a discussion on the sphere radii follows in the next section.) Thus the intercalated Li ion essentially remains ionized in the oxide, while the charge-balancing electron occupies the bottom of the conduction band. This large charge transfer is in sharp contrast to the interaction between the W and O wave functions, where the dominating mechanism in the transferring of electrons to lower energies is hybridization. In general, the occupied part of the conduction band is very similar to that of the pure oxide, implying that a rigid-band filling picture is appropriate. However, the valence band is narrower than in the pure oxide; the bandwidth is reduced from 7.1 eV to 6.4 eV. The band gap, now located in the occupied part of the spectrum, is increased to 1.6 eV.

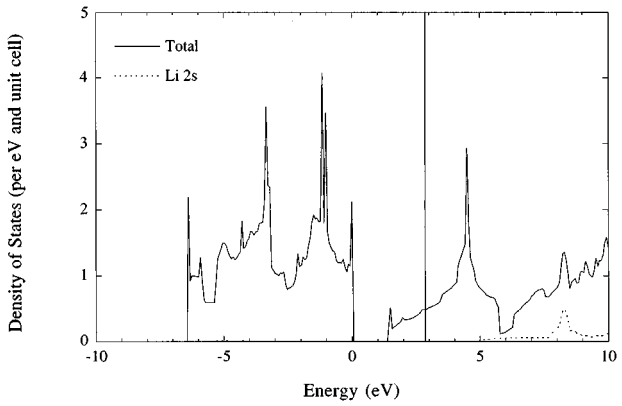

FIG. 6. Density of states for $LiWO_3$. The Li projected state density is included as a dashed curve. The Fermi level is marked as a vertical line.

The calculated equilibrium lattice constant is slightly larger than for the pure oxide, viz., 3.88 Å. This is in contrast to the experimental situation, where it is found that the crystal contracts with increasing Li content, at least up to a concentration of 0.56 Li ions per unit cell, where the contraction is 0.4%.[25]

The charge distribution in real space naturally bears similarity to that of the pure WO_3 material, except for a small peak around the lithium site. Much more illuminating information about the additional electron is found in Fig. 7, where the *difference* in charge density between $LiWO_3$ and WO_3 is presented. The most obvious feature in this figure is the charge that is found around the Li ion [cf. part (b) of the figure]. Other features are the negative difference found near the W and the O cores, showing that the Li ion pulls out the charge slightly compared to the case when it is not present. Around the W sites, the region where electrons are added shows fine structure. Figure 7(b) leads to the conclusion that the charge difference around the O sites extends a considerable distance in space towards the Li ion, and the negative and positive regions appear to cancel in a rough approximation. The charge-balancing additional electron thus seems to occupy the W orbitals pointing diagonally in Fig. 7(a), i.e., with the t_{2g} symmetry expected for the bottom of the conduction band. These conclusions are in agreement with the occupation numbers in Table I, where the O occupation remains almost constant when the Li ion is inserted while the W d occupation increases by 0.2 electrons. The amount of charge in the interstitial region shows the largest increase, quite naturally, from 7.23 to 7.83.

As we will show later (see Sec. III E below) *ab initio* calculations as well as experiments demonstrate that in HWO_3 the hydrogen atom forms a hydroxide unit with an oxygen atom, so the H atom is not positioned at the center of the unit cell. It is therefore of interest to investigate whether the total energy increases or decreases when the lithium atom is moved from the center of the perovskite unit towards one

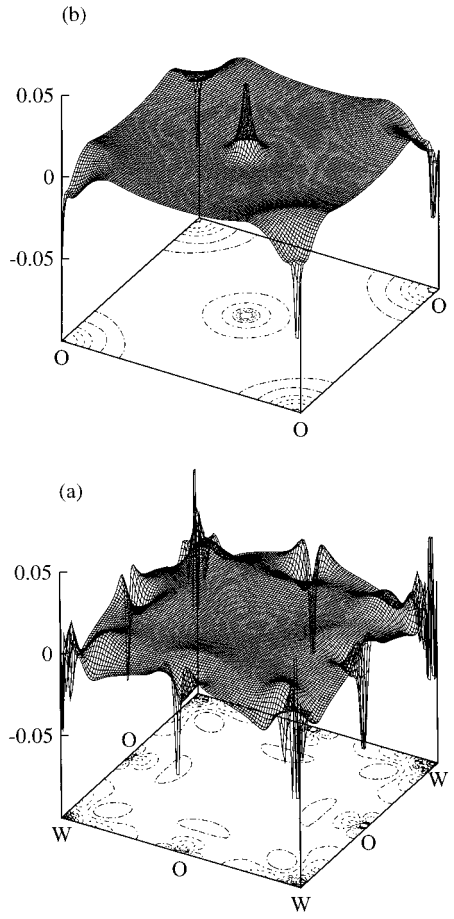

FIG. 7. Difference in charge density between $LiWO_3$ and WO_3, i.e., the density of $LiWO_3$ subtracted by the density for WO_3, for the planes $z=0$ (a) (lower panel) and $z=a/2$ (b) (upper panel), with a being the perovskite lattice parameter. Atomic sites are the same as in Fig. 3, except for the center of (b) where the Li site is found.

of the oxygen atoms. In contrast to the situation for HWO_3, the total energy increases as the ion is moved away from the central position in the unit cell (cf. Fig. 10). Thus we expect the most stable position of the Li site to be centered, which is in agreement with x-ray diffraction data.[25]

D. $NaWO_3$

From a chemical point of view, sodium is very similar to lithium, with almost identical ionization potentials. This similarity is clearly exhibited in the similarity of the density of states plots in Figs. 6 and 8 and in the occupation numbers given in Table I. If we study the difference in charge density between $NaWO_3$ and WO_3, there is no visible difference to the lithium case with regard to the basal plane, whereas the plot for the plane $z=a/2$ reveals that there is one more node in the 3*s* wave function of Na than for the 2*s* function of Li. This slight difference does not affect the calculated properties significantly.

The calculated lattice constant turns out to be the same as for $LiWO_3$, 3.88 Å. The slight increase in lattice constant when Na is incorporated in the system is in agreement with experiments.[3]

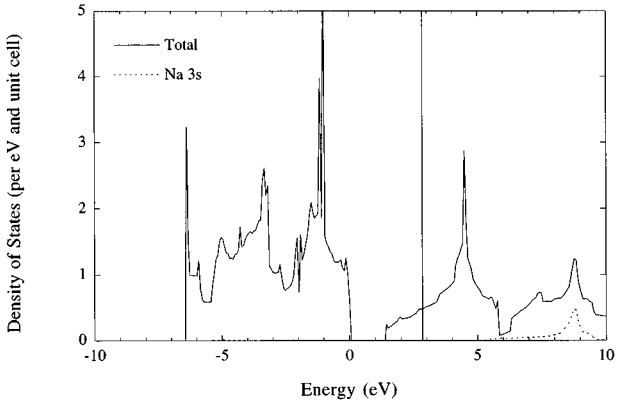

FIG. 8. Density of states for $NaWO_3$. The Na projected state density is included as a dashed curve. The Fermi level is marked as a vertical line.

For $NaWO_3$ we have the possibility to compare with another self-consistent calculation,[12] based on the LMTO method in the atomic spheres approximation. In general, the agreement between the two calculations is excellent. The shape of the valence band as well as the bandwidth agree with angle-resolved photoemission experiments[26] as pointed out in Ref. 12. There is also agreement between the present study and the one by Christensen and Mackintosh[12] as regards the position of the Na peak in the DOS. However, on the low-energy side of the peak they found a considerable contribution to the DOS from the sodium states, a feature not seen in the present work. The labeling of these states as Na states comes from the larger Na sphere in their calculation, 56% of the total volume compared to 11% in the present work. The states that differ among the two calculations occur as interstitial states in the present study. The larger Na sphere size in Ref. 12 also led to a very large occupation number of the Na states, 2.05 electrons, in sharp contrast to the present work where the Na site is occupied with only 0.10 electrons.

For the sake of comparison we have performed a calculation where the Na sphere occupies 38% of the total volume, and in this case the Na occupation increases to 1.22. However, only 0.2 of these states are *s* states and the remaining part is mostly *p* and *d* like. (In Ref. 12 the Na *s* occupation was 0.40 out of 2.05 states.) The conclusion must be that the states with higher angular momenta originate from the tail summation of the orbitals centered on the other atomic sites as well as interstitial states, and the ''true'' sodium occupation, the *s* states, is still quite low. This more or less technical question illustrates the fact that angular momentum is not a well-defined quantity in connection with Bloch theory.

It would be desirable to state the amount of ionicity of the inserted ion, but the results given above do not give support to any reliable conclusion. Further information can be found by studying the shape of the potential between the Na site and a neighboring site. The border between the two atoms could then be defined as the region where the potential is flat. In the calculations reported here, this distance agrees well with the smaller radius used, and thus the statement that the Li or Na site is ionlike is to some extent validated.

E. HWO_3

Hydrogen behaves differently from Li or Na in WO_3. Neutron diffraction data[22] showed that the hydrogen (or deu-

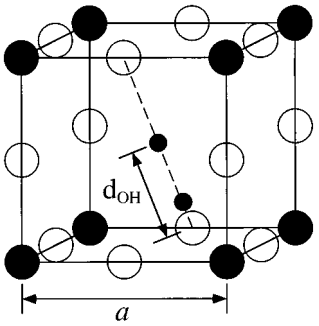

FIG. 9. Unit cell for cubic HWO_3 with the hydrogen atom (small solid circle) located on a line between an oxygen site (empty circle) and the central position. Tungsten sites are marked with solid circles. The distance between the hydrogen and oxygen sites is denoted d_{OH}.

terium) atom is located near an oxygen atom with a maximum distance of 1.1 Å, i.e., that a hydroxide unit is formed. In order to study the hydroxide formation theoretically we performed calculations of total energy as a function of O-H distance (d_{OH}), with the H position being varied from the central position in the perovskite cube along a straight line towards one oxygen atom. The geometry is illustrated in Fig. 9. We find a minimum in total energy for $d_{OH}=1.03$ Å, as shown in Fig. 10. Also shown in the figure is a similar calculation for $LiWO_3$, illustrating that heavier alkali ions favor the central position in the unit cell.

If the calculations are performed using the central position for the hydrogen atom, a large hydrogen-projected state density peak on the Fermi level will result. Such a system supports spin polarization, with a calculated spin polarization energy of ~ 0.5 eV and a total magnetic moment of 0.84 μ_B. However, the total energy of the magnetic state is still larger than for the hydroxide forming state. When d_{OH} is decreased the hydrogen peak moves away from the Fermi level towards higher energies, while a second hydrogen peak originating from the hybridization with the oxygen atom in the OH pair grows at low energies. Focused on the Fermi level, this means that the hydrogen contribution to the state density and the support for spin polarization vanishes as d_{OH} decreases. Figure 11 displays the calculated DOS for the

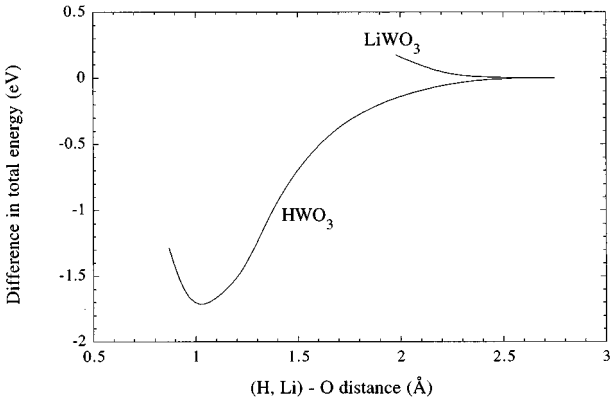

FIG. 10. Total energy for HWO_3 and $LiWO_3$ as a function of distance between H or Li and O atoms, denoted d_{OH} in Fig. 9.

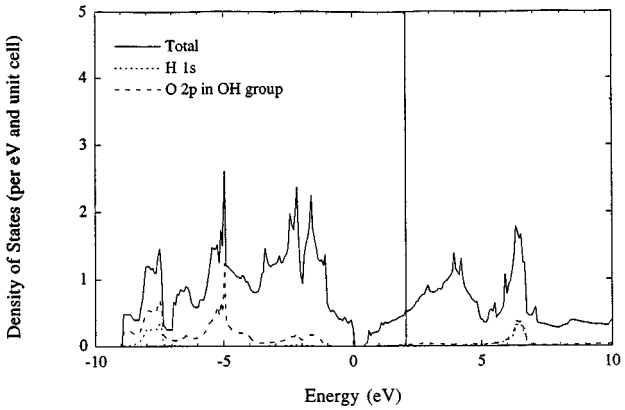

FIG. 11. Density of states for HWO_3 with $d_{OH}=1.03$ Å, corresponding to the minimum in total energy.

hydrogen position where the total energy is minimized. Clearly, the oxygen states in the hydroxide pair are much lowered in energy, thus yielding a broadening of the valence band. The bottom of the conduction band, which now is occupied by one electron, resembles the cases for $LiWO_3$ or $NaWO_3$, and thus the physical properties should not be too different regardless of whether hydrogen or alkali ions are intercalated into the WO_3 host.

Since the hydrogen atom does not occupy the central position, there might be room for more than one hydrogen atom in the crystal. A total energy study of various plausible hydrogen contents shows that the energy gain when one hydroxide unit is formed is 2.6 eV. If an additional hydrogen atom is inserted near an oxygen atom already in a hydroxyl unit, thus forming a water molecule, the energy is lowered with 2.4 eV compared to pure WO_3. On the other hand, if the second hydrogen atom forms another hydroxyl unit, the energy gain is 3.9 eV. From the differences in total energy one can draw the conclusion that the formation of a hydroxide is favored compared to a hydrate (water molecules around the oxygen sits) when hydrogen is inserted into WO_3. From the trends in total energies given above one can predict an energetically favorable uptake of hydrogen until all oxygen atoms participate in hydroxide pairs.

IV. OPTICAL PROPERTIES

The band structure data discussed above lay a good foundation for calculations of different electromagnetic properties of WO_3-based materials intercalated with Li, Na, or H. Below we report some results concerning the optical properties.

The response of a material to electromagnetic radiation depends on many different effects, and it is not the purpose of this work to try to account for them all. We thus concentrate on the interband transitions, and represent intraband contributions in terms of a Drude model. The interband contribution to the imaginary part of the dielectric function, ϵ_2, is calculated by summing transitions from occupied to unoccupied states (with fix **k** vector) over the Brillouin zone, weighted with the matrix element giving the probability for the transition, $\langle \psi_f | \mathbf{p} | \psi_i \rangle$, where i and f denote initial and final states, respectively, and **p** is the momentum operator. ϵ_1 is then found by using Kramers-Kronig relations. The

method of calculation is further described in Ref. 27.

A. WO_3

The optical properties of WO_3 in the visible region are dominated by the absorption threshold, determined by the band gap. For frequencies lower than $E_g/\hbar$, where E_g is the band gap width, the material is essentially transparent, since there are no free electrons present to give a metal-like response, and since interband transitions cannot be excited. When the photon energy is increased and reaches the band gap width, absorption from interband transitions will start to take place. For photon energies slightly larger than E_g (sufficiently large to avoid the Urbach effect[28]) the absorption a can be described by

$$\varepsilon a \propto (\varepsilon - E_g)^{\eta}, \tag{1}$$

where ε is the photon energy and the exponent η depends on the type of optical transition in the gap region. Specifically, η is $\frac{1}{2}$, $\frac{3}{2}$, 2, or 3 for transitions being direct and allowed, direct and forbidden, indirect and allowed, and indirect and forbidden, respectively. Since the top of the valence band is completely dominated by the O p states, while the bottom of the conduction band to 90% is constituted by W d orbitals, the transitions are allowed ($\Delta l = \pm 1$). Furthermore, the band gap is indirect so the exponent η is expected to be 2. Indeed this is in accordance with experiments.[7]

For higher energies, nearer the ultraviolet region, the optical properties are governed by the interband transitions. The reflectance for WO_3, calculated from interband transitions, has a peak around a wavelength corresponding to the onset of transitions across the direct band gap (indirect transitions are neglected in the present study). This effect results in the greenish color of WO_3. As mentioned above, the calculated band gap is smaller than the experimentally determined value, and thus the calculated ''color'' of WO_3 is shifted to longer wavelengths.

B. Li_xWO_3 and Na_xWO_3

The dependence of the optical parameters on the ion content, x, is of importance for reflective electrochromic devices,[7] for example. Performing self-consistent calculations for varying Li or Na content would be extremely time consuming, however, but since a filling of a rigid conduction band seems to be appropriate we approximate the situation of varying ion content simply by adjusting the Fermi level to the desired degree of band filling, using the band structure calculated self-consistently for $x=1$. Using a value of zero for x thus corresponds to pure WO_3, but derived from a calculation for a metallic state ($x=1$). The two curves for this case (derived from Li and Na containing oxide, respectively) are included in Fig. 12. The two curves are not identical, but quite similar, which is a measure of the correctness of the rigid band model. Compared to the reflectance calculated from the self-consistent solution for WO_3 (not presented, cf. the preceding section) the present values show better agreement with experiments since the calculated band gap is larger for the metallic state.

When metallic electrons are present, their contribution to the dielectric function can be approximated by the Drude

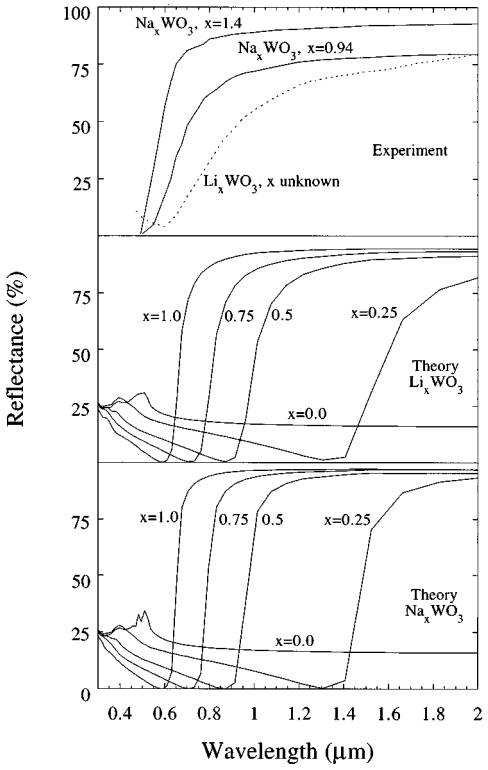

FIG. 12. Reflectance as a function of wavelength for Li_xWO_3 and Na_xWO_3. The upper panel shows experimental data, the middle panel shows calculated data for Li_xWO_3, and the lower panel shows calculated data for Na_xWO_3.

model. This model includes three parameters: the density of conduction electrons, the average relaxation time, and the optical effective mass, m^*. For the present case only the electron density is easy to estimate.

We have chosen to represent the effective mass as the enhancement of the calculated density of states at the Fermi level compared to the density of states from the free-electron model (FEM). In the range $0<x<1$ we thus use the ratio of the calculated DOS to the DOS calculated with the FEM for the corresponding band filling. For both materials this ratio is well approximated by $m^*=1.5$ over the concentration range in interest.

In the FEM, the dc conductivity depends on the ratio of the effective mass to the relaxation time. Starting from the value found for m^* we can thus deduce the relaxation time by comparison with conductivity measurements. Using the values found in Ref. 25 we find the value 9.7×10^{-15} s for the Li containing material, and from Ref. 29 the value 4.8×10^{-14} s is deduced for the corresponding Na compound. Using these values for all concentrations the plasma frequency, and hence the contribution to the dielectric function, will depend only on the electron concentration.

By adjusting the Fermi level to give the electron density corresponding to $x=0$, $x=0.25$, $x=0.5$, $x=0.75$, and $x=1$ we obtain the reflectance curves presented in Fig. 12, middle and lower panels for Li_xWO_3 and Na_xWO_3, respectively. The experimentally determined reflectivity[30] indicates good agreement for high ion concentrations, with an onset in reflectivity at a wavelength of 0.6 to 0.7 μm. In the Na con-

taining material, however, the onset appears at slightly lower wavelengths. For lower electron concentrations the experiments indicate the same onset but gradually lower reflectance, while the calculations give reflectance curves with similar shape but pushed towards longer wavelengths. The calculated curves reach higher reflectivities (above 90%) than the experimental ones do.

The optical properties of ion-intercalated WO_3 have also been studied[31] from the perspective of a dynamic resistivity[32] with ionized impurity scattering accounted for by the Gerlach theory.[33] For low electron concentration one finds that the present theory and the Gerlach theory agree much better with each other than any one of them does with experimental data.

This disagreement between the present work and experiments can be ascribed to several causes. First of all, it is possible that the rigid band filling of the $x=1$ band structure is not sufficiently accurate. However, a comparison of the $x=0$ curve with the self consistent calculation for WO_3 shows only some quantitative differences, and the main features are the same.

Second, polaron absorption might make a non-negligible contribution to the optical properties. Indeed highly disordered WO_3 with intercalated ions exhibit strong polaron absorption in a band centered around a wavelength of 1 μm. Thus polaron absorption is responsible for the absorptive electrochromism in ''amorphous'' tungsten oxide films.[7] With such a contribution superimposed on the curves presented in Fig. 12 one could get better agreement with experiments.

Furthermore, one can imagine that the real material comprises local environments with $x=1$ and $x=0$. By making linear combinations of the two reflectance curves match the desired concentration, one can obtain very good agreement with the experimental data.

V. SUMMARY AND CONCLUSIONS

We have reported *ab initio*, self-consistent calculations (using the local approximation to density functional theory) for the electronic structure of cubic WO_3, hexagonal WO_3, cubic $LiWO_3$, $NaWO_3$, HWO_3, and H_2WO_3. The electronic structure is well described as a filled oxygen p band and a tungsten d band that is empty in WO_3, and gradually filled when hydrogen or alkali ions are inserted, to the degree of band filling that is required by charge-balancing the incorporated ions. During this process the conduction band is fairly rigid.

When the tungsten oxide contains lithium or sodium the alkali dominated band is located 5 eV above the Fermi level, and the occupied part of the spectrum shows very little modification compared to the pure oxide. When hydrogen is inserted into the tungsten oxide, the hydrogen forms hydroxide units with oxygen atoms and thus breaks the symmetry. Hydrogen states are then found both at low and high energies. The low energy peak originates from hybridization with the oxygen states in the hydroxide pair, while the high energy peak constitutes the actual hydrogen level. The bottom of the conduction band is, of course, occupied, and resembles the corresponding part of the electronic structure in the pure oxide.

Thus the insulator-metal transition upon ion insertion is well accounted for. The detailed optical properties, in terms of the dielectric function, have also been calculated using interband transitions (weighted with the proper matrix element) and the Drude model. For larger ion content the agreement with experiment is qualitatively good, but at lower concentrations it is obvious that all effects have not been included in the present theory.

With the present work we have contributed to the understanding of metal oxides and their modifications in electronic properties when other elements are incorporated, which is of fundamental importance in several important technologies presently under vigorous development.

ACKNOWLEDGMENTS

Valuable discussions with Professor Börje Johansson and Dr. Olle Eriksson are acknowledged. Parts of the calculations were performed at the Swedish National Supercomputing Centre in Linköping.

[1] J.J. Berzelius, Afhandlingar i Fysik, Kemi och Mineralogie **4**, 293 (1815); J. Chem. Phys. (Berlin) (also referred to as Schweigger's Journal) **16**, 476 (1816).

[2] F. Wöhler, Ann. Phys. **2**, 350 (1824).

[3] B.W. Brown and E. Banks, J. Am. Chem. Soc. **76**, 963 (1954).

[4] J.B. Goodenough, in *Progress in Solid State Chemistry*, edited by H. Reiss (Pergamon, Oxford, 1971), Vol. 5, pp. 145–399.

[5] N. Kobosew and N.I. Nekrassow, Z. Elektrochem. **36**, 529 (1930).

[6] E.O. Brimm, J.C. Brantley, J.H. Lorentz, and M.H. Jellinek, J. Am. Chem. Soc. **73**, 5427 (1951).

[7] C. G. Granqvist, *Handbook of Inorganic Electrochromic Materials* (Elsevier, Amsterdam, 1995).

[8] P. M. S. Monk, R. J. Mortimer, and D. R. Rosseinsky, *Electrochromism: Fundamentals and Applications* (VCH Verlagsgesellschaft, Weinheim, 1995).

[9] L. F. Mattheiss, Phys. Rev. B **2**, 3918 (1970).

[10] D. W. Bullett, Solid State Commun. **46**, 575 (1983); J. Phys. C **16**, 2197 (1983).

[11] C. G. Zhan and F. Zheng, J. Mol. Struct. **285**, 89 (1993).

[12] N. E. Christensen and A. R. Mackintosh, Phys. Rev. B **35**, 8246 (1987).

[13] P. Hohenberg and W. Kohn, Phys. Rev. **136**, B846 (1964); W. Kohn and L. J. Sham, *ibid.* **140**, A1133 (1965); L. Hedin and B. I. Lundqvist, J. Phys. C **4**, 2064 (1971); O. Gunnarsson and B. I. Lundqvist, Phys. Rev. B **13**, 4274 (1976).

[14] U. von Barth and L. Hedin, J. Phys. C **5**, 1629 (1972); J. F. Janak, V. L. Moruzzi, and A. R. Williams, Phys. Rev. B **12**, 1257 (1975).

[15] J. M. Wills (unpublished); J. M. Wills and B. R. Cooper, Phys. Rev. B **36**, 3809 (1987); D. L. Price and B. R. Cooper, *ibid.* **39**, 4945 (1989).

[16] H. L. Skriver, *The LMTO Method* (Springer-Verlag, Berlin, 1984); O. K. Andersen, Phys. Rev. B **12**, 3060 (1975).
[17] D. D. Koelling and B. N. Harmon, J. Phys. C **10**, 3107 (1977).
[18] D. J. Chadi and M. L. Cohen, Phys. Rev. B **8**, 5747 (1973); S. Froyen, *ibid.* **39**, 3168 (1989).
[19] M. Figlarz, Prog. Solid State Chem. **19**, 1 (1989).
[20] W. Sahle and M. Nygren, J. Solid State Chem. **48**, 154 (1983).
[21] T. Nanba and I. Yasui, J. Solid State Chem. **83**, 304 (1989); T. Nanba, Y. Nishiyama, and I. Yasui, J. Mater. Res. **6**, 1324 (1991); T. Nanba, T. Takahashi, S. Takano, J. Takada, A. Osaka, Y. Miura, T. Kudo, and I. Yasui, J. Ceram. Soc. Jpn. **103**, 222 (1995).
[22] P. J. Wiseman and P. G. Dickens, J. Solid State Chem. **6**, 374 (1973).
[23] Q. Zhong, J. R. Dahn, and K. Colbow, Phys. Rev. B **46**, 2554 (1992).
[24] See, e.g., M. Hybertsen and S. G. Louie, Comments Condens. Matter Phys. **13**, 5 (1987).
[25] M. E. Straumanis and S. S. Hsu, J. Am. Chem. Soc. **72**, 4027 (1950); M. J. Sienko and T. B. N. Truong, *ibid.* **83**, 3939 (1961).
[26] H. Höchst, R. D. Bringans, and H. R. Shanks, Phys. Rev. B **26**, 1702 (1982).
[27] J. M. Wills (unpublished).
[28] F. Urbach, Phys. Rev. **92**, 1324 (1953).
[29] B. W. Brown and E. Banks, Phys. Rev. **84**, 609 (1951).
[30] F. O. Arntz, R. B. Goldner, B. Morel, T. E. Haas, and K. K. Wong, J. Appl. Phys. **67**, 3177 (1990); S. F. Cogan, T. D. Plante, M. A. Parker, and R. D. Rauh, Solar Energy Mater. **14**, 185 (1986); J. Appl. Phys. **60**, 2735 (1986); R. B. Goldner, G. Berrera, F. O. Arntz, T. E. Haas, B. Morel, and K. K. Wong, in *Electrochromic Materials*, edited by M. K. Carpenter and D. A. Corrigan (The Electrochemical Society, Pennington, 1990), Vol. 90-2, p. 14.
[31] J. S. E. M. Svensson and C. G. Granqvist, Appl. Phys. Lett. **45**, 828 (1984).
[32] M. G. Calkin and P. J. Nicholson, Rev. Mod. Phys. **39**, 361 (1967).
[33] E. Gerlach, J. Phys. C **19**, 4585 (1986).